processes

MDPI

Article

Exploring Different Designs in Thieno[3,4-*b*]pyrazine-Based Dyes to Enhance Divergent Optical Properties in Dye-Sensitized Solar Cells

Daniele Franchi [1,*], Matteo Bartolini [1], Francesco D'Amico [1,2], Massimo Calamante [1,3], Lorenzo Zani [1], Gianna Reginato [1], Alessandro Mordini [1,3] and Alessio Dessì [1,*]

[1] Institute of Chemistry of Organometallic Compounds (CNR-ICCOM), Via Madonna del Piano 10, I-50019 Sesto Fiorentino, Italy; mbartolini@iccom.cnr.it (M.B.); francesco.damico@iccom.cnr.it (F.D.); massimo.calamante@iccom.cnr.it (M.C.); lorenzo.zani@iccom.cnr.it (L.Z.); gianna.reginato@iccom.cnr.it (G.R.); alessandro.mordini@iccom.cnr.it (A.M.)

[2] Department of Biotechnology, Chemistry and Pharmacy, University of Siena, Via A. Moro 2, I-53100 Siena, Italy

[3] Department of Chemistry "U. Schiff", University of Florence, Via della Lastruccia 13, I-50019 Sesto Fiorentino, Italy

* Correspondence: daniele.franchi@iccom.cnr.it (D.F.); alessio.dessi@iccom.cnr.it (A.D.); Tel.: +39-055-5225205 (A.D.)

Abstract: Two novel organic sensitizers for Dye-Sensitized Solar Cells (DSSC), called **TP1** and **TP2**, based on the electron-poor thieno[3,4-*b*]pyrazine (TPz) π-bridge and the electron-rich *N*,*N*-bis(4-(hexylthio)phenyl)aniline (TPA) were designed following two different approaches: the classical D-A-π-A design and a symmetric structure with double anchoring functions. Both compounds were prepared exploiting short synthetic pathways based on direct arylation strategies and possibly *one-pot* desymmetrization. The two novel dyes displayed opposite optical properties: a broad and intense light absorption over the entire visible spectrum for **TP1**, and a localized absorption that peaked in the center of the visible region for **TP2**, resulting in a pitch-dark coloration and a green tone, respectively. When assembling the photovoltaic devices, different electrolyte compositions were explored to enhance the optical properties of the dyes. Power conversion efficiencies as high as 5.2% under full sun intensity were recorded for small test devices. The composition of the light transmitted through the **TP2**-containing transparent DSSC fits well with the human eye sensitivity spectrum, thus fulfilling the transparency requirements for building-integrated photovoltaics (BIPV).

Keywords: Dye-Sensitized Solar Cells; thieno[3,4-*b*]pyrazine; dyes; building-integrated photovoltaics

Citation: Franchi, D.; Bartolini, M.; D'Amico, F.; Calamante, M.; Zani, L.; Reginato, G.; Mordini, A.; Dessì, A. Exploring Different Designs in Thieno[3,4-*b*]pyrazine-Based Dyes to Enhance Divergent Optical Properties in Dye-Sensitized Solar Cells. *Processes* **2023**, *11*, 1542. https://doi.org/10.3390/pr11051542

Academic Editor: Chiing-Chang Chen

Received: 21 April 2023
Revised: 12 May 2023
Accepted: 15 May 2023
Published: 17 May 2023

1. Introduction

The recent rise in energy prices, together with the ever-growing worldwide energy demand and the shortage of supplies of non-renewable fuels, such as coal, oil, and natural gas, are unassailable reasons which should prompt us to complete the energy transition to renewable and low-impact energy sources as soon as possible. Even the construction industry is starting to realize that a general image of sustainability is not enough, and the aim of zero-energy buildings must be pursued for all new constructions. Photovoltaics should represent one of the leading technologies driving the transition process thanks to the abundance and wide distribution of solar energy. To accomplish this goal, it is necessary to make buildings self-sufficient from an energy point of view through the development of building-integrated photovoltaics (BIPV) [1–4].

To maximize energy production using BIPV, it would be desirable to take advantage of all the available surfaces in a building, including those designated to receive lighting from the outside, such as windows or glass walls. However, many of the device properties required for such an application, such as semi-transparency, tunable color,

and interior visual comfort, are not intrinsic to the classic silicon-based photovoltaic technology, nor they are used in other emerging technologies, such as organic photovoltaics and perovskite solar cells (PSCs) [5,6]. In particular, attention must be paid to the human eye spectral sensitivity, which is not equally distributed along the entire solar spectrum but is centered in the green region at a maximum wavelength of 555 nm under daylight conditions [7]. Technical solutions which fulfill this requirement for BIPV (i.e., average visible transmittance (AVT) > 20%) are already available, such as the employment of amorphous silicon-based (a-Si) solar cells, though the price to pay is a significant reduction in terms of efficiency (≈7%) [8]. On the other hand, among the emerging photovoltaic technologies, Dye-Sensitized Solar Cells (DSSCs) distinguish themselves for their high versatility in terms of color palette and transparency level, having the ideal properties required for an application in the BIPV field, together with the use of non-toxic materials [9].

Optimizing each DSSC component can contribute to enhancing the transparency of the device. Moon et al. [10] substituted the usual diffusive scattering layer with a two-dimensional photonic crystal reflector to maintain high photon-to-electric conversion efficiency (8.23%), but with a significantly higher perceived transparency (52% vs. 0.3%) of the photoanode. Magnesium-doped tin oxide was demonstrated to be a conductive material with higher optical transparency (>80%) than indium-doped tin oxide, as well as good electrical conductivity (421.15 Ω/cm), and was used as a conducting substrate for the fabrication of DSSC [11]. Counter electrodes based on various conducting polymers, such as poly(3,4-ethylenedioxythiophene) (PEDOT) [12] or polyaniline (PANI) [13], can also be used to enhance the perceived transparency without affecting the photovoltaic efficiency of the DSSC device.

However, while modifications of glass substrates, semiconductor, and counter electrode can enhance the light transmittance in the overall visible spectrum, the human eye spectral sensitivity can be enhanced selectively only through modulating the light absorption spectrum of the DSSC photosensitizer. A possible approach is to use a dye cocktail in which two dyes with complementary light absorption properties, found in the UV and the NIR regions, respectively, sensitize the same photoanode to maintain high energy conversion efficiencies and transmit the light only in the intermediate wavelength range. This strategy was pursued by Han et al. [14], who combined the NIR-absorbing squaraine-based dye HSQ5 with the UV-absorbing dye Y1, obtaining green-colored DSSC devices with a maximum light transmittance of 60.3% in the 500–600 nm region and a photon-to-current efficiency of 3.66%. Hagar et al. [15] investigated the theoretical and experimental photo-electrochemical properties of a series of novel diimide and Schiff base UV-absorbers with carboxyl and pyridyl anchoring groups, evaluating their potential co-sensitization with the NIR-absorber VG20 in transparent DSSC. On the other side, Sauvage et al. [16] optimized the structure of a polymethine cyanine-based dye (VG20-C_{16}) to absorb only near-infrared light beyond 700 nm: the resulting colorless DSSC devices displayed a 3.1% power conversion efficiency and a remarkable average visible transmittance of up to 76%.

In the last few years, our research group gained significant experience in the design and synthesis of novel organic dyes for DSSC with light absorption properties tailored to reach high visible transparency [17,18] or attain specific colorations [19,20]. Moreover, we recently prepared a series of thieno[3,4-*b*]pyrazine-based molecules (TPz) as potential fluorophores in Luminescent Solar Concentrators (LSCs), which showed maximum absorbance well above 500 nm and a higher transmittance in the intermediate wavelength range [21,22]. Similar light absorption properties were displayed by the DSSC dyes featuring the TPz core recently reported by Delcamp et al. [23–25]. For this reason, we supposed that the TPz core could be used as the starting point to design novel organic dyes with optical properties highly compatible with the human eye sensitivity spectrum. In particular, we designed compound **TP1** with an unsymmetric D-A-π-A structure and **TP2** bearing a D-A-D structure and two anchoring moieties on the central core (Figure 1). In both cases, to modulate the photo-electrochemical properties of the dyes, we chose to introduce the *N*,*N*-*bis*(4-(hexylthio)phenyl)aniline as the donor group, since it was demonstrated to

enhance dye regeneration and increase DSSC open circuit potential (V_{OC}) compared to its oxygenated analog [26,27].

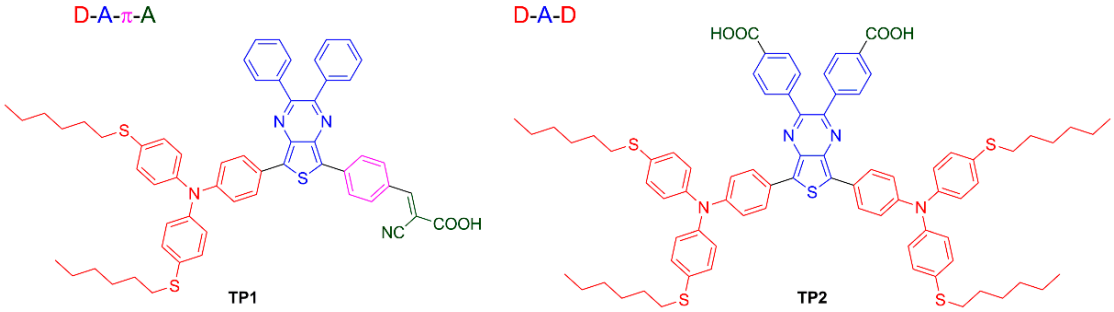

Figure 1. Structures of new photosensitizers **TP1–2**.

Spectroscopic characterization of the resulting dyes showed divergent optical properties, which were selectively exploited to provide DSSC test devices with different predominant features: either enhanced photovoltaic performances, in the case of the more panchromatic absorber (**TP1**), or improved perceived transparency for that with the most localized absorption profile (**TP2**).

2. Materials and Methods

2.1. General Information

Unless otherwise stated, all reagents were purchased from commercial suppliers and used without purification. 2,3-diphenylthieno[3,4-*b*]pyrazine (**1**) [21], 4-bromo-*N*,*N*-*bis*(4-(hexylthio)phenyl)aniline (**2**) [26], and thiophene-3,4-diamine (**8**) [21] were prepared as previously reported. All air-sensitive reactions were performed using Schlenk techniques. Solvents used in cross-coupling reactions were previously degassed using the "freeze-pump-thaw" method. Toluene was dried on a resin exchange Solvent Purification System (MBraun), and ethanol was distilled over magnesium. Petroleum ether, unless specified, was the 40–70 °C boiling fraction. Reactions were monitored via TLC using silica gel 60 F254 aluminum sheet (Merck); the detection was made using a $KMnO_4$ basic solution or UV lamp. Flash column chromatography was performed using glass columns (10–50 mm wide) and Silica Gel 60 (230–400 mesh). ^{1}H- and ^{13}C-NMR spectra were recorded at 400 and 100.6 MHz, respectively, on Bruker Avance series instruments. Chemical shifts were referenced to the residual solvent peak ($CDCl_3$, δ 7.26 ppm for ^{1}H-NMR and δ 77.16 ppm for ^{13}C-NMR; CD_2Cl_2, δ 5.32 ppm for ^{1}H-NMR and δ 53.84 ppm for ^{13}C-NMR; THF-d_8 δ, 1.72 and 3.58 ppm for ^{1}H-NMR, δ 67.21 and 25.31 ppm for ^{13}C-NMR). Coupling constants (*J*) were reported in Hz. ESI-MS analyses were recoded with LCQ-Fleet Ion-Trap Mass Spectrometer (Thermo Fisher Scientific Italy, Milan, Italy). HR-MS analyses were performed at CISM (Mass Spectrometry Center—University of Florence) using an LTQ Orbitrap FT- MS Spectrometer (Thermo). FT-IR spectra were recorded with a Perkin-Elmer Spectrum BX instrument in the range 4000–400 cm^{-1} with a 2 cm^{-1} resolution. UV-Vis spectra in different solvents were recorded on diluted solutions of the analyte (approximately 10^{-5} M) with a Shimadzu UV-2600 spectrometer. UV-Vis absorption or transmittance spectra of the compounds adsorbed on TiO_2 were recorded with the same instrument in transmission mode after the sensitization of thin, transparent semiconductor films (thickness approximately 5 μm). Fluorescence spectra in solution were measured at room temperature with a Jasco FP-8300 spectrofluorometer equipped with a 450 W Xenon arc lamp.

2.2. Synthesis

2.2.1. Synthesis of 4-(7-(4-(bis(4-(Hexylthio)phenyl)amino)phenyl)-2,3-diphenylthieno[3,4-b]pyrazin-5-yl)benzaldehyde (**4**)

TPz **1** (66 mg, 0.23 mmol, 1.0 eq.), $Pd(OAc)_2$ (2.6 mg, 0.011 mmol, 5.0 mol%), P(*t*-Bu)$_3$HBF$_4$ (6.6 mg, 0.023 mmol, 10 mol%), pivalic acid (12 mg, 0.11 mmol, 50 mol%), Cs_2CO_3 (0.112 g, 0.34 mmol, 1.5 eq.) and bromide **2** (0.108 g, 0.19 mmol, 0.85 eq.) were dissolved in toluene (1.0 mL). The reaction mixture was stirred for 2.5 h at 90 °C; 4-bromobenzaldehyde (**3**, 85 mg, 0.46 mmol, 2.0 eq.) and an additional portion of Cs_2CO_3 (0.112 g, 0.34 mmol, 1.5 eq.) were then added. The resulting mixture was stirred for 5 h at 100 °C, before being cooled down to room temperature and filtered over Celite®. The filter cake was washed with chloroform (30 mL), and the organic phase was washed with brine (30 mL). After anhydrification over Na_2SO_4, filtration, and evaporation of the solvent under vacuum, the crude was purified via flash column chromatography (toluene) to afford pure **4** (42 mg, 0.052 mmol, 21% yield) as a dark purple solid. ^{1}H–NMR (400 MHz, CD_2Cl_2): δ = 9.97 (s, 1H), 8.48 (d, *J* = 8.4 Hz, 2H), 8.18 (d, *J* = 8.8 Hz, 2H), 7.91 (d, *J* = 8.4 Hz, 2H), 7.54 (d, *J* = 7.3 Hz, 2H), 7.49 (d, *J* = 7.0 Hz, 2H), 7.29–7.41 (m, 6H), 7.26 (d, *J* = 8.4 Hz, 4H), 7.10 (d, *J* = 8.8 Hz, 2H), 7.07 (d, *J* = 8.4 Hz, 4H), 2.91 (t, *J* = 7.3 Hz, 4H), 1.66 (q, *J* = 7.3 Hz, 4H), 1.38–1.48 (m, 4H), 1.28–1.35 (m, 8H), 0.90 (t, *J* = 6.8 Hz, 6H) ppm; ^{13}C–NMR{1H} (100 MHz, CD_2Cl_2): δ = 191.8, 153.9, 153.0, 148.2, 145.5, 140.8, 139.8, 139.7, 139.1, 135.21, 135.17, 132.3, 131.0, 130.6, 130.4, 130.3, 129.6, 129.4, 129.3, 128.7, 128.6, 127.9, 127.7, 127.2, 125.9, 125.6, 123.1, 34.7, 31.9, 29.8, 29.0, 23.1, 14.4 ppm; ESI–MS: *m*/*z* = 867.3 $[M]^+$.

2.2.2. Synthesis of (E)-3-(4-(7-(4-(bis(4-(Hexylthio)phenyl)amino)phenyl)-2,3-diphenylthieno[3,4-b]pyrazin-5-yl)phenyl)-2-cyanoacrylic Acid (TP1)

Aldehyde **4** (45 mg, 0.052 mmol, 1.0 eq.) was reacted with cyanoacetic acid (13 mg, 0.155 mmol, 3.0 eq.) and piperidine (31 mg, 36 µL, 0.364 mmol, 3.0 eq.) in $CHCl_3$ (2.0 mL) for 8 h at 80 °C; the heating was then interrupted. The reaction mixture was diluted with $CHCl_3$ (20 mL) and washed with $HCl_{(aq.)}$ 0.3 M (20 mL); after anhydrification of the organic phase over Na_2SO_4, the solvent was removed under vacuum. The crude was purified through washing with portions of ethanol (2 × 10 mL) and pentane (2 × 10 mL), affording **TP1** in pure form (41 mg, 0.044 mmol, 84% yield) as a green–black solid. ^{1}H–NMR (400 MHz, THF-d_8): δ = 8.59 (d, *J* = 8.4 Hz, 2H), 8.27–8.36 (m, 2H), 8.25 (s, 1H), 8.16 (d, *J* = 8.4 Hz, 2H), 7.57 (d, *J* = 6.6 Hz, 2H), 7.53 (d, *J* = 7.7 Hz, 2H), 7.20–7.41 (m, 11H), 7.04–7.15 (m, 5H), 2.92 (t, *J* = 7.3 Hz, 4H), 1.65 (q, *J* = 7.3 Hz, 4H), 1.41–1.51 (m, 4H), 1.29–1.37 (m, 8H), 0.87–0.93 (m, 6H) ppm; ^{13}C–NMR{1H} (100 MHz, THF-d_8): δ = 163.8, 154.3, 153.5, 153.4, 148.6, 145.8, 141.2, 140.2, 140.1, 139.5, 138.8, 135.1, 132.9, 132.2, 131.2, 130.6, 130.5, 129.6, 129.5, 128.7, 128.6, 128.0, 127.6, 126.8, 126.1, 124.3, 124.2, 123.1, 116.4, 103.3, 34.5, 32.2, 30.0, 29.2, 23.3, 14.2 ppm; HRMS (ESI): *m*/*z* calculated for $C_{58}H_{55}N_4O_2S_3$: 935.34817 $[M]^+$. Found: 935.34815.

2.2.3. Synthesis of Dimethyl 4,4′-(1-Hydroxy-2-oxoethane-1,2-diyl)dibenzoate (**6**) [28]

Thiamine hydrochloride (0.24 g, 0.71 mmol, 5.0 mol%.) was dissolved in a H_2O:MeOH = 1:3 mixture (8.7 mL) and a 2.0 M solution of aqueous NaOH (0.6 mL) was added dropwise at 0 °C. The colorless solution turned bright yellow, and methyl 4-formylbenzoate (**5**) (2.00 g, 12.18 mmol, 1.00 eq.) was added. The suspension was heated to 80 °C and stirred for 1 h. The reaction mixture was cooled down to RT and quenched with H_2O (6.0 mL) to precipitate the product (**6**) as a white solid, which was filtered and washed with H_2O and MeOH (1.56 g, 4.75 mmol, 78% yield). Spectroscopic data were in agreement with those already reported [28]. ^{1}H–NMR (400 MHz, $CDCl_3$) δ = 8.01 (d, *J* = 8.4 Hz, 2H), 7.94 (d, *J* = 8.3 Hz, 2H), 7.90 (d, *J* = 8.4 Hz, 2H), 7.38 (d, *J* = 8.3 Hz, 2H), 6.00 (s, 1H), 4.60 (br, 1H), 3.87 (s, 3H), 3.83 (s, 3H) ppm; ^{13}C–NMR{1H} (100 MHz, $CDCl_3$) δ = 198.3, 166.4, 165.8, 143.1, 136.7, 134.7, 130.5, 129.9, 129.0, 127.8, 76.2, 52.6, 52.3 ppm.

2.2.4. Synthesis of Dimethyl 4,4′-Oxalyldibenzoate (**7**) [29]

In a round-bottom flask equipped with a reflux condenser, benzoin derivative **6** (1.56 g, 4.75 mmol, 1.0 eq.) was dissolved in DMSO (26.7 mL), and HBr 48% (9.34 mL, 8.25 mmol, 1.74 eq.) was added. The yellow solution was stirred for 16 h at 55 °C, and the reaction progress was controlled via TLC (PE:EtOAc = 1:1). The bright yellow suspension was cooled down to RT, quenched with H_2O (50.0 mL), and filtered. The bright yellow precipitate was suspended in H_2O and filtered again to afford product **7** (1.53 g, 4.70 mmol, 99% yield), with no need for further purification. Spectroscopic data were in agreement with those already reported [29]. ^{1}H–NMR (400 MHz, $CDCl_3$) δ = 8.18 (d, *J* = 7.5 Hz, 4H), 8.05 (d, *J* = 7.4 Hz, 4H), 3.96 (s, 6H) ppm; ^{13}C–NMR{1H} (100 MHz, $CDCl_3$) δ = 193.0, 166.0, 135.9, 135.7, 130.3, 130.0, 52.8 ppm.

2.2.5. Synthesis of Dimethyl 4,4′-(Thieno[3,4-*b*]pyrazine-2,3-diyl)dibenzoate (**9**) [30]

Oxalyldibenzoate (**7**) (0.15 g 0.46 mmol, 1.00 eq.) and thiophene-3,4-diamine (**8**) (54 mg, 0.48 mmol, 1.05 eq.) were dissolved in dry EtOH (4.0 mL) under an inert atmosphere of N_2. The resulting suspension was stirred and refluxed under an inert atmosphere for 16 h, monitoring the reaction progress via TLC (PE:EtOAc = 1:1). The resulting dark green suspension was cooled down to RT and filtered off. The solid was washed with EtOH and purified via short column chromatography (gradient from DCM to DCM:MeOH = 100:1) to obtain **9** (0.145 g, 0.36 mmol, 78% yield) as a dark green powder. Spectroscopic data were in agreement with those already reported [30]. ^{1}H–NMR (400 MHz, $CDCl_3$) δ = 8.13 (s, 2H), 7.98 (d, *J* = 8.0 Hz, 4H), 7.50 (d, *J* = 8.1 Hz, 4H), 3.92 (s, 6H) ppm; ^{13}C–NMR{1H} (100 MHz, $CDCl_3$) δ = 166.7, 152.1, 143.2, 141.6, 130.6, 129.8, 129.7, 118.5, 52.4 ppm.

2.2.6. Synthesis of Dimethyl 4,4′-(5,7-bis(4-(bis(4-(Hexylthio)phenyl)amino)phenyl)thieno[3,4-*b*]pyrazine-2,3-diyl)dibenzoate (**10**) [21]

TPz **9** (30 mg, 0.07 mmol, 1.00 eq.), bromide **2** (103 mg, 0.17 mmol, 2.50 eq.), $Pd(OAc)_2$ (2.4 mg, 0.01 mmol, 15 mol%), $P(tBu)_3HBF_4$ (6 mg, 0.02 mmol, 30 mol%), Cs_2CO_3 (84 mg, 0.25 mmol, 3.7 eq.), and pivalic acid (3.7 mg, 0.036 mmol, 50 mol%) were dissolved in dry *N*,*N*-DMF (0.3 mL). The brown mixture was warmed up to 90 °C and maintained under magnetic stirring for 16 h, during which time the reaction progress was monitored via TLC (PE:EtOAc = 4:1). The dark blue mixture was diluted with DCM, filtered on Silica gel, and purified via flash column chromatography (gradient from PE:DCM = 1.1 to pure DCM) to obtain the desired product **10** (69 mg, 0.05 mmol, 73% yield) as a dark green solid. ^{1}H–NMR (400 MHz, THF-d_8) δ = 8.25 (d, *J* = 8.8 Hz, 4H), 7.95 (d, *J* = 8.3 Hz, 4H), 7.62 (d, *J* = 8.3 Hz, 4H), 7.27 (d, *J* = 8.6 Hz, 8H), 7.11 (d, *J* = 8.8 Hz, 4H), 7.06 (d, *J* = 8.6 Hz, 8H), 3.85 (s, 6H), 2.91 (t, *J* = 7.3 Hz, 8H), 1.69–1.60 (m, 8H), 1.52–1.39 (m, 8H), 1.36–1.28 (m, 18H), 0.90 (t, *J* = 6.8 Hz, 12H) ppm; ^{13}C–NMR{1H} (100 MHz, THF-d_8) δ = 166.7, 152.3, 148.4, 146.3, 144.7, 139.4, 132.9, 131.7, 131.6, 130.9, 130.2, 129.5, 128.4, 126.2, 123.8, 52.3, 34.9, 32.5, 30.4, 29.5, 23.6, 14.5 ppm.

2.2.7. Synthesis of 4,4′-(5,7-bis(4-(bis(4-(Hexylthio)phenyl)amino)phenyl)thieno[3,4-*b*]pyrazine-2,3-diyl)dibenzoic acid (**TP2**) [24]

Ester **10** (55 mg, 0.04 mmol, 1.00 eq.) was dissolved in THF (20.0 mL), and a freshly prepared 2 M solution of $LiOH{\cdot}H_2O$ in MeOH (20.0 mL) was added. The dark green thick solution was stirred vigorously for 2 h at RT. The resulting dark blue mixture was poured into ice-cold water, and the dark blue suspension was neutralized with a 3 M HCl aqueous solution till pH = 5, at which point a blue precipitate formed. The solid was recovered via filtration and washed with water, affording the desired product **TP2** (44 mg, 0.03 mmol, 83% yield) as a dark green solid. ^{1}H–NMR (400 MHz, THF-d_8) δ = 8.24 (d, *J* = 8.6 Hz, 4H), 7.96 (d, *J* = 8.2 Hz, 4H), 7.60 (d, *J* = 8.2 Hz, 4H), 7.27 (d, *J* = 8.5 Hz, 8H), 7.10 (d, *J* = 8.6 Hz, 4H), 7.06 (d, *J* = 8.4 Hz, 8H), 2.91 (t, *J* = 7.3 Hz, 8H), 1.69–1.60 (m, 8H), 1.49–1.40 (m, 8H), 1.37–1.27

(m, 16H), 0.90 (t, J = 6.7 Hz, 12H) ppm; ^{13}C–NMR{1H} (100 MHz, THF-d_8) δ = 167.3, 152.4, 148.3, 146.3, 144.4, 139.4, 132.8, 132.2, 131.6, 130.8, 130.4, 129.5, 128.5, 126.2, 123.8, 34.9, 32.5, 30.4, 29.5, 23.6, 14.6 ppm; HRMS (ESI): m/z calculated for $C_{80}H_{87}N_4O_4S_5$: 1327.53254 $[M]^+$. Found: 1327.53135.

3. Results and Discussion

3.1. Synthesis of the Dyes

The synthetic pathways followed to prepare the two dyes are reported in Scheme 1. The synthesis of dye **TP1** required the employment of diphenyl-substituted TPz **1** and 4-bromo-*N*,*N*-*bis*(4-(hexylthio)phenyl)aniline (**2**), which were prepared as previously reported by our group [21,26]. Thus, TPz **1** was subjected to a one-pot double arylation reaction (DA) to break the symmetry of the molecule and introduce the donor group (via reaction with **2**) and, after that, the acceptor group (via reaction with commercially available bromide **3**). The reaction conditions (stoichiometric ratio of the reagents, the choice of pre-catalyst, ligand, and base, as well as temperature and time) were adapted from our previous reports of one-pot DA reactions for the construction of other DSSC dyes [19,20], allowing us to isolate the desired D-A-π-A intermediate **4** with a 21% overall yield. The overall synthesis was carried out in just one step, resulting in a much shorter sequence and a reduced production of waste in comparison with classic cross-coupling protocols, such as Suzuki–Miyaura and Stille–Migita reactions [31].

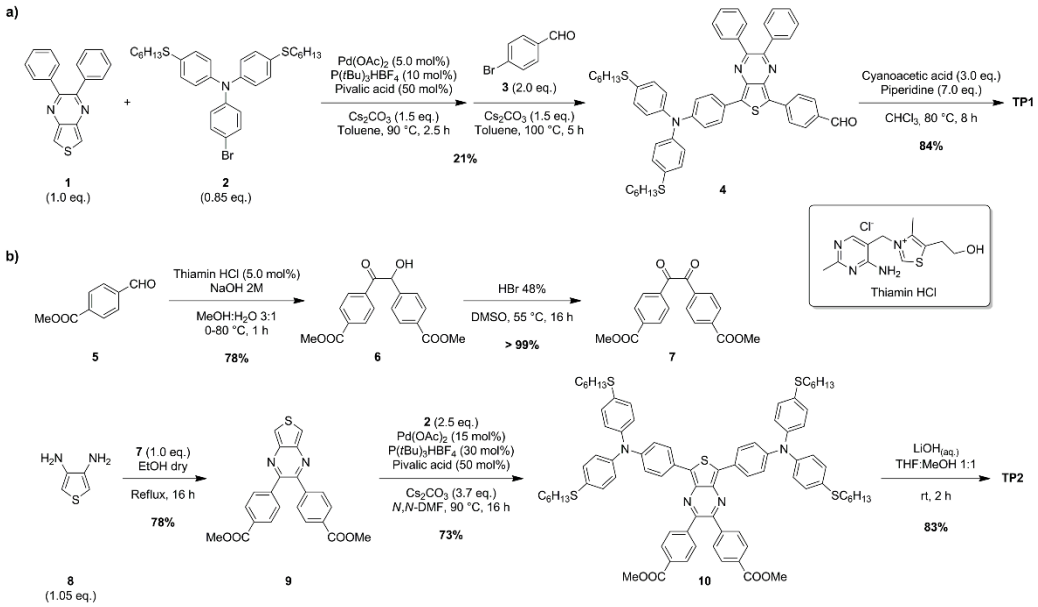

Scheme 1. Synthesis of dyes **TP1** (**a**) and **TP2** (**b**).

Regarding the preparation of **TP2**, access to 1,2-diketone **7** was required, since it is not commercially available. Unlike the process reported in the literature [32], we were not able to prepare **7** via palladium-catalyzed cross-coupling on vinylene carbonate acting as a synthetic equivalent of glyoxal; therefore, some alternative routes were investigated. Initially, we attempted a cyanide-free benzoin umpolung self-condensation of commercially available methyl 4-formylbenzoate (**5**) in a basic environment. When the reaction was catalyzed with ionic liquid BMII, using ultrasounds to obtain a homogeneous solution [33,34], the desired product **6** was obtained. Unfortunately, this process yielded unreproducible yields ranging from 6 to 81%, probably due to the non-homogeneity of the ultrasounds mixing method. On the other hand, the thiamin-catalyzed cyanide-free benzoin condensation of benzoate **5** gave more reproducible results, producing the desired α-hydroxyketone **6** in good yield [28]. Acid-catalyzed oxidation of compound **6** with DMSO gave the desired dicarbonyl intermediate **7** in quantitative yield [29,35]. Condensation of **7** with diamine **8**

in dry ethanol afforded TPz **9** with high yield, followed by a DA with bromide **2**, carrying the donor group, while quantitative ester hydrolysis under basic conditions allowed us to isolate dye **TP2** in 83% yield. The yield of the overall five-step **TP2** synthesis is 36%.

3.2. Spectroscopic and Electrochemical Characterization of Dyes **TP1–2**

Both dyes **TP1** and **TP2** were completely characterized from a spectroscopic and electrochemical point of view (see Table 1). Firstly, UV-Vis spectra of the dyes were recorded in $CHCl_3$ solvent (conc. $\approx 10^{-5}$ M; Figure 2a,b). **TP1** solution showed a dark purple color and almost panchromatic light absorption, with three main peaks: the first one was centered in the green region of the spectrum (λ_{max} = 572 nm), and the other two were located in the blue (λ_{max} = 420 nm) and UV (λ_{max} = 337 nm) regions. Molar attenuation coefficients (ε) of the peaks in the visible region fall in the 1.8–1.9 $\times$ 10^4 M^{-1} cm^{-1} range, while the UV-absorption intensity is higher (ε = 4.10 $\times$ 10^4 M^{-1} cm^{-1}). **TP2** solution is characterized by a green coloration, due to a fairly intense absorption peak in the 500–700 nm region (λ_{max} = 597 nm, ε = 3.70 $\times$ 10^4 M^{-1} cm^{-1}) and a broad UV-Vis band (λ < 450 nm) with a high molar attenuation coefficient, up to 3.0 $\times$ 10^5 M^{-1} cm^{-1}. These light absorption properties were confirmed through the transmittance spectra of the semi-transparent thin-layer TiO_2 electrodes (thickness: 5 µm) dyed with **TP1** and **TP2** (Figure 2c), with relative minimum transparencies in the visible region, i.e., among 550 and 600 nm and below 400 nm. The overlay with the CIE photopic spectral luminous efficiency function [36], which represents the average spectral sensitivity of human visual perception of light, showed a significant overlapping with the transmittance spectrum of **TP1**, while **TP2** exhibited a much better matching. The average visible light transmission (*AVT*) through the photoanode was calculated based on the following equation: [37]

$$AVT(\%) = \frac{\int_{390}^{830} T(\lambda) \times V(\lambda) \times S(\lambda) d\lambda}{\int_{390}^{830} V(\lambda) \times S(\lambda) d\check{}}$$

where $T(\lambda)$ is the transmission of the sample, $V(\lambda)$ is the photopic spectral luminous efficiency function, and $S(\lambda)$ is the AM 1.5 g solar spectrum (ASTM G-173 Global 37 Deg Tilt standard) [38]. While **TP1** photoanode reached 42.3% *AVT*, **TP2** showed a very high *AVT* of 83.7%, thus appearing as a very promising candidate as a photosensitizer for highly transparent DSSCs in BIPV. This trend in *AVT* values could be in contrast with the fact that **TP2** has a molar attenuation coefficient (ε) in solution larger than that of **TP1**. The explanation for such opposite behavior can be found in the mismatch of the light absorption spectra of **TP2** and the human eye sensitivity $V(\lambda)$, while **TP1** has a maximum absorption that perfectly matches with $V(\lambda)$. Moreover, it is worth noticing that, despite a larger molar attenuation coefficient in solution, the **TP2** transmittance on the TiO_2 layer is higher than that of **TP1**. This discrepancy could be related to a lower amount of dye anchored onto the semiconductor surface, since each rigid dicarboxylic **TP2** molecule occupies at least double as many active sites of the semiconductor layer with respect to **TP1**.

To complete the spectroscopic characterization, Tauc plots were drawn, starting from the UV-Vis data in $CHCl_3$ solution (Figures S1 and S2) to estimate the optical bandgaps (E_{0-0}) of the dyes, whose values were equal to 1.91 and 1.82 eV for **TP1** and **TP2** respectively, confirming their ability to also absorb light in the visible/near-IR regions. Cyclic voltammetries (CV) of dyes **TP1** and **TP2** were recorded in CH_2Cl_2 and THF solutions, respectively, using 0.1 M $TBAPF_6$ as supporting electrolyte and ferrocene as internal standard [39] to evaluate the oxidation potentials of the dyes at both the ground and excited states (see Figures S3 and S4, and Table 1). Both molecules showed quasi-reversible first oxidation peaks and very similar ground-state oxidation potentials (E_{ox}), which were equal to 1.01 and 1.04 V for **TP1** and **TP2,** respectively. These values should be positive enough to guarantee dye regeneration by the most common redox couples, such as I^-/I_3^-, $Co^{2+/3+}$, and $Cu^{+/2+}$ complexes. Excited-state oxidation potentials (E_{ox}*) were obtained subtracting E_{0-0} to E_{ox}; while the −0.90 V value calculated for **TP1** should be negative enough to ensure

a fast electron injection into the TiO_2 conduction band, **TP2** exhibited a lower E_{ox}* (−0.78 V), which could make the electron transfer from the excited state of the dye more troublesome (see Figure S5) [40,41].

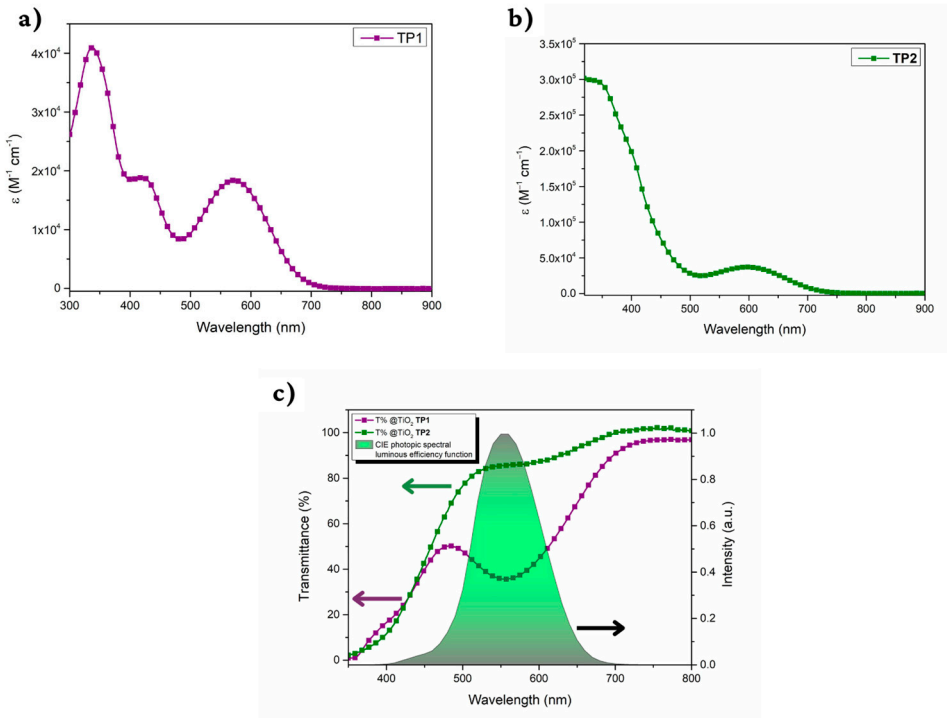

Figure 2. UV-Vis light absorption spectra of dyes **TP1** (**a**) and **TP2** (**b**) in $CHCl_3$ solution (conc. ≈ 10^{-5} M). (**c**) Transmittance spectra of semi-transparent thin-layer TiO_2-based electrodes photosensitized with dyes **TP1–2** and comparison with the CIE photopic spectral luminous efficiency function.

Table 1. Spectroscopic and electrochemical data of dyes **TP1** and **TP2**.

	λ_{abs} [nm] ($\varepsilon \times 10^4$ [M^{-1} cm^{-1}]) [a]	λ_{abs} on TiO_2 [nm]	AVT [%]	E_{0-0} [eV] [b]	E_{ox} [V] [c]	E_{ox}* [V] [d]
TP1	572 (1.83); 420 (1.88); 337 (4.10)	557	42.3	1.91	1.01	–0.90
TP2	597 (3.70); 306 (30.49)	591	83.7	1.82	1.04	–0.78

[a] In $CHCl_3$ solution. [b] Calculated from Tauc plots. [c] Working electrode: glassy carbon; counter-electrode: platinum; reference electrode: Ag/$AgNO_3$ 0.01 M in MeCN; supporting electrolyte: $TBAPF_6$ 0.1 M in DCM (**TP1**) or THF (**TP2**); ferrocene as the internal standard [40]. Values are reported against NHE. [d] E_{ox}* = E_{ox}. − E_{0-0}.

3.3. Photovoltaic Characterization of Dyes **TP1–2**

The prepared dyes **TP1–2** were employed as sensitizers in the construction of small DSSC test devices to evaluate their photovoltaic properties. All the details on the device construction are reported in the supplementary information (see Section S4). Aiming for devices with high perceived transparency, all prepared samples featured a thin semi-transparent screen-printed layer of TiO_2 as the semiconductor for the photoanode and a semitransparent screen-printed Pt layer as the cathode.

The prepared dyes and a reference compound (**TTZ5**, Figure S6) previously reported by our group [42] were tested together with the commercially available iodine-based electrolyte solution EL-HSE (GreatCell Solar, entries labeled HSE in Table 2 and Figure 3a). Aiming again for high-transparency devices, other electrolytic solutions characterized by a weaker visible light absorption spectrum and/or a lower molar attenuation coefficient were also tested (entries labeled LIE in Table 2 and Figure 3a). In particular, an electrolyte solution with low-iodine content [43] was formulated via mixing iodide salts with no

iodine (details on the electrolyte formulation are reported in Section S4). Indeed, a low amount of iodine, which was necessary to collect charges at the cathode, was produced in situ using the photo-oxidated dye once the DSSC devices were assembled and exposed to simulated sunlight. Despite that, the overall transparency of the device was preserved and a remarkable transmittance value, higher than 30% in almost the whole visible spectrum, was obtained for a test DSSC device containing the **TP2** dye and the LIE electrolyte (see Figure S7).

Table 2. Photovoltaic characterization of DSSC devices sensitized with **TP1–2** or reference dye **TTZ5** and featuring iodine-based electrolytes.

Dye	Electrolyte	J_{SC} [mA cm^{-2}]	V_{OC} [mV]	*ff* [%]	η [%]
TP1	HSE	10.38 ± 0.27	680 ± 6	73.0 ± 0.5	5.16 ± 0.12
	LIE	8.44 ± 0.48	695 ± 9	72.5 ± 2.9	4.24 ± 0.04
TP2	HSE	8.67 ± 0.41	680 ± 5	68.4 ± 1.4	4.03 ± 0.14
	LIE	6.97 ± 0.38	689 ± 3	69.6 ± 1.5	3.35 ± 0.19
TTZ5	HSE	14.08	711	74.4	7.44
	LIE	13.48	751	69.0	6.98

All devices were measured two days after construction. Values for **TP1–2** samples are reported as average of three samples with their standard deviation.

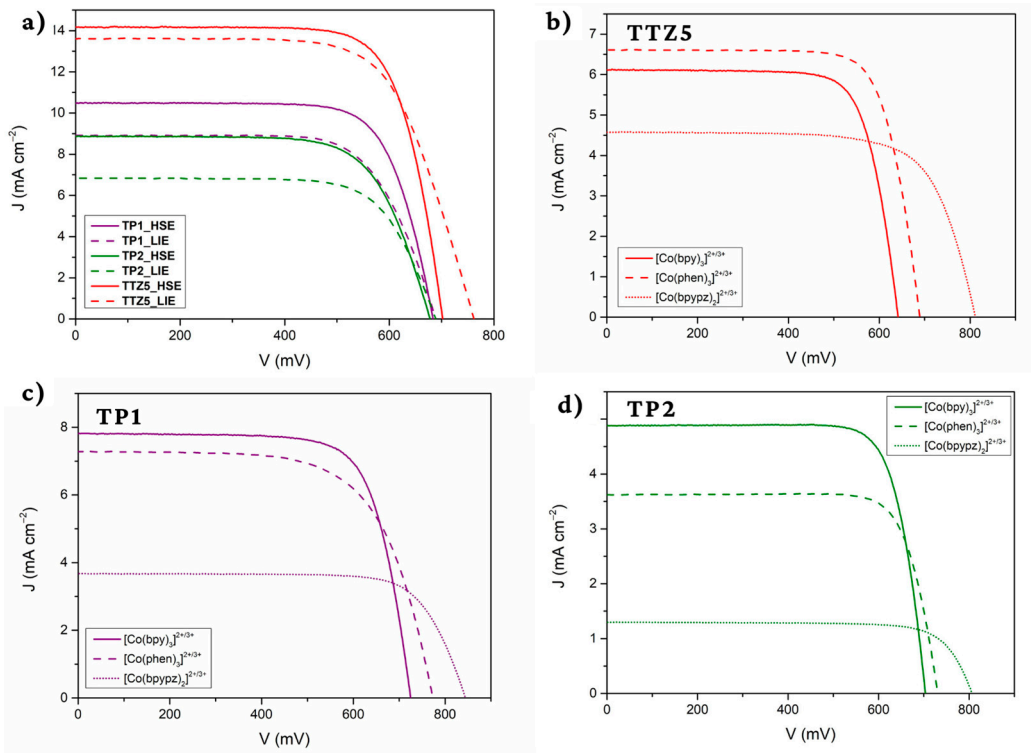

Figure 3. J/V curves of photovoltaic test devices (active area = 0.25 cm^2) under 1 Sun AM 1.5 G irradiance. (**a**) Comparison of different dyes in combination with a commercially available iodine-based electrolyte (HSE) or a highly transparent low-iodine-containing electrolyte (LIE). Devices featuring electrolytes based on different cobalt complexes and sensitized with (**b**) **TTZ5**, (**c**) **TP1**, or (**d**) **TP2**.

The photovoltaic performances of all devices improved constantly for a few days, during which time it is believed the electrolytes intercalated into the mesoporous structure of the semiconductor and a small amount of iodine (triiodide) was produced in situ in the low-iodine content electrolyte to further improve device efficiency. Table 2 and Figure 3a

report the photovoltaic characterization on the second day after device construction, and clearly show how all samples benefit from the use of the low-iodine content electrolyte, in terms of not only transparency but also V_{OC}. This behavior is in line with a lower concentration of the oxidized species in the electrolyte, making its redox potential more positive and, thus, enlarging its gap compared to the Fermi level of the semiconductor, which correlates with the V_{OC} of the device. On the other hand, the short-circuit photocurrent density (J_{SC}) decreases when replacing HSE with LIE electrolyte, probably due to the mass transport limitation [43]. Interestingly, the changes in J_{SC} and power conversion efficiency (η%) across different dyes follow the same trend of the light-harvesting properties of the dyes employed. Despite the loss in terms of η%, which was limited to 16–17% of the initial efficiency value for **TP1–2**, the employment of the LIE electrolyte can be encouraged for BIPV applications; this finding is especially relevant when **TP2** is used as the dye, since the increment in terms of device transparency is remarkable (see Figure S7). To quantify such added value, we recorded the transparency of the active area of full devices sensitized with **TP2** and calculated an AVT value of 27.5% when using HSE as the electrolyte, compared to 36.9% when using LIE. The product between AVT and η is best known as the light utilization efficiency (LUE) and can be used to better evaluate the photovoltaic device, simultaneously taking into account both the perceived transparency and the energy conversion efficiency [37]. The LUE value for **TP2**-HSE was computed to be 1.42, while **TP2**-LIE devices reached 1.57, proving that the gained transparency justifies the slight loss in power conversion efficiency.

Furthermore, dyes **TP1–2** and the reference sensitizer **TTZ5** were also tested with three electrolyte solutions based on cobalt complexes with bi- and tri-dentate nitrogen-containing the following ligands: [44,45] 2,2′-bipyridine ($Co(bpy)_3$), phenanthroline ($Co(phen)_3$), and 6-(3,5-dimethylpyrazol-1-yl)-2,2′-bipyridine ($Co(pzbpy)_2$) (Figure 4). The corresponding J/V curves are reported in Figure 3b–d.

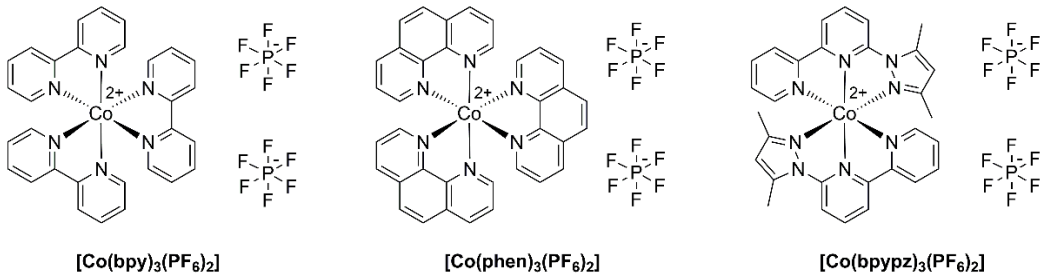

Figure 4. Structures of three cobalt (II)-based complexes employed in this work.

Other than a light absorption spectrum located almost only in the UV region (see Figure S8), such electrolytes are also characterized by progressively more positive redox potentials (0.565, 0.614, and 0.767 V vs. NHE respectively) and were, therefore, anticipated to enhance the V_{OC} of the devices. Indeed, as shown in Table 3, the expected progressive increase in V_{OC} moving from $Co(bpy)_3$ to $Co(pzbpy)_2$ was observed, but was also accompanied by a relevant loss in J_{SC}, which was generally attributed to a slower regeneration reaction due to a lower driving force for the reaction [46]. In fact, while **TP1** features the well-established D-A-π-A structure, which is known to separate the photoinduced charges efficiently, therefore stunting the TiO_2-dye charge recombination, **TP2** instead has a branched symmetrical D-A-D structure that seems to be less efficient in separating the charges and, when used in combination with electrolytes with a very low regeneration overpotential, gives rise to TiO_2-dye recombination phenomena with a rate that is competitive with the one of dye–electrolyte regeneration. Similarly, the potential of $Co(pzbpy)_2$ seems to be excessively positive, leading to dye regeneration and/or charge recombination issues for both **TP1–2**. This issue is particularly evident with **TP2**, whose drop in photovoltaic efficiency is solely imputable to a drastic reduction in J_{SC}, which is symptomatic of slow dye regeneration. Interestingly, when used with $Co(phen)_3$ transparent electrolyte,

dye **TP1** still shows good power conversion efficiencies of 4%, overcoming the reference compound **TTZ5**.

Table 3. Photovoltaic characterization of DSSC devices fabricated with dyes **TP1–2** or reference sensitizer **TTZ5** and three cobalt-based electrolytes.

Dye	Electrolyte	J_{SC} [mA cm^{-2}]	V_{OC} [mV]	*ff* [%]	η [%]
TP1	$Co(bpy)_3$	7.37 ± 0.52	706 ± 8	75.3 ± 1.8	4.00 ± 0.30
	$Co(phen)_3$	7.20 ± 0.44	770 ± 3	72.4 ± 4.4	4.01 ± 0.36
	$Co(bpypz)_2$	3.55 ± 0.15	844 ± 1	73.6 ± 3.0	2.21 ± 0.13
TP2	$Co(bpy)_3$	4.58 ± 0.21	721 ± 6	75.9 ± 3.7	2.46 ± 0.18
	$Co(phen)_3$	3.59 ± 0.15	731 ± 4	77.5 ± 3.3	2.03 ± 0.05
	$Co(bpypz)_2$	1.20 ± 0.19	806 ± 11	78.3 ± 1.4	0.75 ± 0.10
TTZ5	$Co(bpy)_3$	6.13 ± 0.32	640 ± 7	74.5 ± 1.5	2.92 ± 0.08
	$Co(phen)_3$	6.71 ± 0.45	697 ± 14	75.1 ± 1.0	3.51 ± 0.32
	$Co(bpypz)_2$	4.64 ± 0.29	817 ± 8	72.1 ± 2.0	2.74 ± 0.27

All devices were measured two days after construction. Values for **TP1–2** samples are reported as average of three samples with their standard deviation.

4. Conclusions

In this work, two novel thieno[3,4-*b*]pyrazine-based organic sensitizers **TP1–2** for DSSC were synthesized, characterized, and tested for photovoltaic performance. **TP1** features a D-A-π-A design, while **TP2** has a symmetric structure with double anchoring functions. The dyes displayed divergent optical properties: **TP1** has a broad and intense light absorption in the whole visible spectrum, resulting in an average transparency (AVT) equal to 42.3%, while **TP2** presents two localized absorption bands with AVT of 83.7%, suggesting, therefore, a feasible application in BIPV. Cells built with **TP1–2** show appreciable photovoltaic performance with iodide-based electrolytes (5.16% and 4.03%, respectively), and the transparency of the whole devices could be improved through exploiting transparent electrolytes with low-iodine formulations, at the cost of a slight efficiency loss (less than 20%). Tests with cobalt-based electrolytes, i.e., $Co(bpy)_3$, $Co(phen)_3$, and $Co(pzbpy)_2$, highlighted a limited compatibility of **TP1–2** with redox couples characterized by potentials as high as that of $Co(pzbpy)_2$ (0.767 V vs. NHE). On the other hand, devices showed a large gain in V_{OC} compared to those built with the triiodide/iodide-based electrolytes, especially in the case of **TP1**, which, in combination with $Co(phen)_3$ reached a PCE of 4.01% with a V_{OC} of 770 mV, overcoming the reference dye **TTZ5** in the same transparent configuration.

Supplementary Materials: The following supporting information can be downloaded at: https://www.mdpi.com/article/10.3390/pr11051542/s1, Figure S1: Tauc plot of the dye **TP1** in $CHCl_3$ solution; Figure S2: Tauc plot of the dye **TP2** in $CHCl_3$ solution; Figure S3: Cyclic Voltammetry of dye **TP1** in CH_2Cl_2 solution; Figure S4: Cyclic Voltammetry of dye **TP2** in THF solution; Figure S5: Energy level diagram of ground-state and excited-state oxidation potentials of dyes **TP1-2**; Figure S6: Molecular structure of the reference dye **TTZ5**; Figure S7: Transmittance spectra of the whole semi-transparent cells containing **TP-2** and different electrolytes (HSE and LIE); Figure S8: UV-Vis light absorption spectra of the three cobalt-based electrolyte solutions $Co(bpy)_3$, $Co(phen)_3$, and $Co(bpypz)_2$.; Section S1: Tauc plots for TP1-2; Section S2: Cyclic voltammetry for TP1-2; Section S3: TP1-2 energy levels; Section S4: DSSC assembly and efficiency measurements; Section S5: Copies of ^{1}H and ^{13}C-NMR spectra. References [47–50] are cited in the supplementary materials.

Author Contributions: Conceptualization, A.D.; synthesis and characterization, D.F., A.D. and M.C.; Photovoltaic investigation, F.D. and M.B.; writing—original draft preparation, D.F. and A.D.; writing—review and editing, A.D., D.F., L.Z. and M.C.; funding acquisition, A.M. and G.R. All authors have read and agreed to the published version of the manuscript.

Funding: This research was funded by MASE PTR22-24, project "Fotovoltaico ad Alta Efficienza". M.B. is grateful for the research grant provided within the Regione Toscana project "VINCI- fotoVoltaico INnovativo per appliCazione Indoor". F.D. is grateful for the Ph.D. grant within the PON/DM 1061/2021 project "New photosensitive materials for photovoltaic cells operating in low-light conditions and IoT devices".

Institutional Review Board Statement: Not applicable.

Informed Consent Statement: Not applicable.

Data Availability Statement: Not applicable.

Acknowledgments: The authors thank Lucio Cinà (Cicci Research S.R.L.) for providing technical support.

Conflicts of Interest: The authors declare no conflict of interest.

References

1. Pillai, D.S.; Shabunko, V.; Krishna, A. A comprehensive review on building integrated photovoltaic systems: Emphasis to technological advancements, outdoor testing, and predictive maintenance. *Renew. Sustain. Energy Rev.* **2022**, *156*, 111946. [CrossRef]
2. Kirimtat, A.; Tasgetiren, M.F.; Brida, P.; Krejcar, O. Control of PV integrated shading devices in buildings: A review. *Build. Environ.* **2022**, *214*, 108961. [CrossRef]
3. Ikudayisi, A.E.; Chan, A.P.; Darko, A.; Adegun, O.B. Integrated design process of green building projects: A review towards assessment metrics and conceptual framework. *J. Build. Eng.* **2022**, *50*, 104180. [CrossRef]
4. Abdalazeem, M.E.; Hassan, H.; Asawa, T.; Mahmoud, H. Review on integrated photovoltaic-green roof solutions on urban and energy-efficient buildings in hot climate. *Sustain. Cities Soc.* **2022**, *82*, 103919. [CrossRef]
5. Almora, O.; Baran, D.; Bazan, G.C.; Cabrera, C.I.; Erten-Ela, S.; Forberich, K.; Guo, F.; Hauch, J.; Ho-Baillie, A.W.Y.; Jacobsson, T.J.; et al. Device Performance of Emerging Photovoltaic Materials (Version 3). *Adv. Energy Mater.* **2023**, *13*, 2203313. [CrossRef]
6. Almora, O.; Baran, D.; Bazan, G.C.; Berger, C.; Cabrera, C.I.; Catchpole, K.R.; Erten-Ela, S.; Guo, F.; Hauch, J.; Ho-Baillie, A.W.Y.; et al. Device Performance of Emerging Photovoltaic Materials (Version 2). *Adv. Energy Mater.* **2021**, *11*, 2102526. [CrossRef]
7. Gross, H.; Blechinger, F.; Achtner, B. *Handbook of Optical Systems: Volume 4: Survey of Optical Instruments*; Wiley-VCH: Weinheim, Germany, 2012; Volume 4; ISBN 978-3-527-40380-6.
8. Lim, J.W.; Shin, M.; Lee, D.J.; Lee, S.H.; Yun, S.J. Highly transparent amorphous silicon solar cells fabricated using thin absorber and high-bandgap-energy n/i-interface layers. *Sol. Energy Mater. Sol. Cells* **2014**, *128*, 301–306. [CrossRef]
9. Muñoz-García, A.B.; Benesperi, I.; Boschloo, G.; Concepcion, J.J.; Delcamp, J.H.; Gibson, E.A.; Meyer, G.J.; Pavone, M.; Pettersson, H.; Hagfeldt, A.; et al. Dye-sensitized solar cells strike back. *Chem. Soc. Rev.* **2021**, *50*, 12450–12550. [CrossRef]
10. Baek, S.; Ha, S.-J.; Lee, H.; Kim, K.; Kim, D.; Moon, J.H. Monolithic Two-Dimensional Photonic Crystal Reflectors for the Fabrication of Highly Efficient and Highly Transparent Dye-Sensitized Solar Cells. *ACS Appl. Mater. Interfaces* **2017**, *9*, 37006–37012. [CrossRef]
11. Kiruthiga, G.; Rajni, K.S.; Raguram, T.; Eswaramoorthy, N.; Pitchaiya, S. Indium-free $MgSnO_3$ transparent conductive oxide layer: Investigation on structural, optical and electrical properties and photovoltaic performance analysis. *Appl. Nanosci.* **2022**, *13*, 3421–3434. [CrossRef]
12. Gao, S.; Lan, Z.; Wu, W.; Que, L.; Wu, J.; Lin, J. Room temperature polymerization of poly(3,4-ethylenedioxythiophene) as transparent counter electrodes for dye-sensitized solar cells. *Polym. Adv. Technol.* **2014**, *25*, 1560–1564. [CrossRef]
13. Jeon, S.S.; Kim, C.; Lee, T.H.; Lee, Y.W.; Do, K.; Ko, J.; Im, S.S. Camphorsulfonic Acid-Doped Polyaniline Transparent Counter Electrode for Dye-Sensitized Solar Cells. *J. Phys. Chem. C* **2012**, *116*, 22743–22748. [CrossRef]
14. Zhang, K.; Qin, C.; Yang, X.; Islam, A.; Zhang, S.; Chen, H.; Han, L. High-Performance, Transparent, Dye-Sensitized Solar Cells for See-Through Photovoltaic Windows. *Adv. Energy Mater.* **2014**, *4*, 1301966. [CrossRef]
15. Alnoman, R.B.; Nabil, E.; Parveen, S.; Hagar, M.; Zakaria, M.; Hasanein, A.A. Synthesis and Computational Characterization of Organic UV-Dyes for Cosensitization of Transparent Dye-Sensitized Solar Cells. *Molecules* **2021**, *26*, 7336. [CrossRef]
16. Naim, W.; Novelli, V.; Nikolinakos, I.; Barbero, N.; Dzeba, I.; Grifoni, F.; Ren, Y.; Alnasser, T.; Velardo, A.; Borrelli, R.; et al. Transparent and Colorless Dye-Sensitized Solar Cells Exceeding 75% Average Visible Transmittance. *JACS Au* **2021**, *1*, 409–426. [CrossRef]
17. Franchi, D.; Calamante, M.; Coppola, C.; Mordini, A.; Reginato, G.; Sinicropi, A.; Zani, L. Synthesis and Characterization of New Organic Dyes Containing the Indigo Core. *Molecules* **2020**, *25*, 3377. [CrossRef] [PubMed]
18. Dessì, A.; Sinicropi, A.; Mohammadpourasl, S.; Basosi, R.; Taddei, M.; De Biani, F.F.; Calamante, M.; Zani, L.; Mordini, A.; Bracq, P.; et al. New Blue Donor–Acceptor Pechmann Dyes: Synthesis, Spectroscopic, Electrochemical, and Computational Studies. *ACS Omega* **2019**, *4*, 7614–7627. [CrossRef]
19. Dessì, A.; Calamante, M.; Sinicropi, A.; Parisi, M.L.; Vesce, L.; Mariani, P.; Taheri, B.; Ciocca, M.; Di Carlo, A.; Zani, L.; et al. Thiazolo[5,4-*d*]thiazole-based organic sensitizers with improved spectral properties for application in greenhouse-integrated dye-sensitized solar cells. *Sustain. Energy Fuels* **2020**, *4*, 2309–2321. [CrossRef]

20. Dessì, A.; Chalkias, D.A.; Bilancia, S.; Sinicropi, A.; Calamante, M.; Mordini, A.; Karavioti, A.; Stathatos, E.; Zani, L.; Reginato, G. D–A–π–A organic dyes with tailored green light absorption for potential application in greenhouse-integrated dye-sensitized solar cells. *Sustain. Energy Fuels* **2021**, *5*, 1171–1183. [CrossRef]
21. Goti, G.; Calamante, M.; Coppola, C.; Dessì, A.; Franchi, D.; Mordini, A.; Sinicropi, A.; Zani, L.; Reginato, G. Donor-Acceptor-Donor Thienopyrazine-Based Dyes as NIR-Emitting AIEgens. *Eur. J. Org. Chem.* **2021**, *2021*, 2655–2664. [CrossRef]
22. Yzeiri, X.; Calamante, M.; Dessì, A.; Franchi, D.; Pucci, A.; Ventura, F.; Reginato, G.; Zani, L.; Mordini, A. Synthesis and Spectroscopic Characterization of Thienopyrazine-Based Fluorophores for Application in Luminescent Solar Concentrators (LSCs). *Molecules* **2021**, *26*, 5428. [CrossRef] [PubMed]
23. Liyanage, N.P.; Yella, A.; Nazeeruddin, M.; Grätzel, M.; Delcamp, J.H. Thieno[3,4-*b*]pyrazine as an Electron Deficient π-Bridge in D–A−π–*A* DSCs. *ACS Appl. Mater. Interfaces* **2016**, *8*, 5376–5384. [CrossRef] [PubMed]
24. Peddapuram, A.; Cheema, H.; Adams, R.E.; Schmehl, R.H.; Delcamp, J.H. A Stable Panchromatic Green Dual Acceptor, Dual Donor Organic Dye for Dye-Sensitized Solar Cells. *J. Phys. Chem. C* **2017**, *121*, 8770–8780. [CrossRef]
25. Cheema, H.; Peddapuram, A.; Adams, R.E.; McNamara, L.; Hunt, L.A.; Le, N.; Watkins, D.L.; Hammer, N.I.; Schmehl, R.H.; Delcamp, J.H. Molecular Engineering of Near Infrared Absorbing Thienopyrazine Double Donor Double Acceptor Organic Dyes for Dye-Sensitized Solar Cells. *J. Org. Chem.* **2017**, *82*, 12038–12049. [CrossRef] [PubMed]
26. Dessì, A.; Calamante, M.; Mordini, A.; Peruzzini, M.; Sinicropi, A.; Basosi, R.; de Biani, F.F.; Taddei, M.; Colonna, D.; Di Carlo, A.; et al. Organic dyes with intense light absorption especially suitable for application in thin-layer dye-sensitized solar cells. *Chem. Commun.* **2014**, *50*, 13952–13955. [CrossRef]
27. Robson, K.C.D.; Hu, K.; Meyer, G.J.; Berlinguette, C.P. Atomic Level Resolution of Dye Regeneration in the Dye-Sensitized Solar Cell. *J. Am. Chem. Soc.* **2013**, *135*, 1961–1971. [CrossRef]
28. Guo, B.; Li, F.; Wang, C.; Zhang, L.; Sun, D. A rare (3,12)-connected zirconium metal–organic framework with efficient iodine adsorption capacity and pH sensing. *J. Mater. Chem. A* **2019**, *7*, 13173–13179. [CrossRef]
29. Medabalmi, V.; Ramanujam, K. Introduction of Carbonyl Groups: An Approach to Enhance Electrochemical Performance of Conjugated Dicarboxylate for Li-Ion Batteries. *J. Electrochem. Soc.* **2017**, *164*, A1720–A1725. [CrossRef]
30. McNamara, L.E.; Liyanage, N.; Peddapuram, A.; Murphy, J.S.; Delcamp, J.H.; Hammer, N.I. Donor–Acceptor–Donor Thienopyrazines via Pd-Catalyzed C–H Activation as NIR Fluorescent Materials. *J. Org. Chem.* **2015**, *81*, 32–42. [CrossRef]
31. Parisi, M.L.; Dessì, A.; Zani, L.; Maranghi, S.; Mohammadpourasl, S.; Calamante, M.; Mordini, A.; Basosi, R.; Reginato, G.; Sinicropi, A. Combined LCA and Green Metrics Approach for the Sustainability Assessment of an Organic Dye Synthesis on Lab Scale. *Front. Chem.* **2020**, *8*, 214. [CrossRef]
32. Kim, K.H.; Park, B.R.; Lim, J.W.; Kim, J.N. An efficient palladium-catalyzed synthesis of benzils from aryl bromides: Vinylene carbonate as a synthetic equivalent of glyoxal. *Tetrahedron Lett.* **2011**, *52*, 3463–3466. [CrossRef]
33. Garapati, V.K.R.; Gravel, M. Oxazolium Salts as Organocatalysts for the Umpolung of Aldehydes. *Org. Lett.* **2018**, *20*, 6372–6375. [CrossRef]
34. Estager, J.; Lévêque, J.-M.; Turgis, R.; Draye, M. Neat benzoin condensation in recyclable room-temperature ionic liquids under ultrasonic activation. *Tetrahedron Lett.* **2007**, *48*, 755–759. [CrossRef]
35. Li, C.; Xu, Y.; Lu, M.; Zhao, Z.; Liu, L.; Zhao, Z.; Cui, Y.; Zheng, P.; Ji, X.; Gao, G. A Novel and Efficient Oxidation of Benzyl Alcohols to Benzaldehydes with DMSO Catalyzed by Acids. *Cheminform* **2002**, *34*, 2041–2042. [CrossRef]
36. Sharpe, L.T.; Stockman, A.; Jagla, W.; Jägle, H. A luminous efficiency function, VD65* (λ), for daylight adaptation: A correction. *Color Res. Appl.* **2011**, *36*, 42–46. [CrossRef]
37. Traverse, C.J.; Pandey, R.; Barr, M.C.; Lunt, R.R. Emergence of highly transparent photovoltaics for distributed applications. *Nat. Energy* **2017**, *2*, 849–860. [CrossRef]
38. Reference Air Mass 1.5 Spectra | Grid Modernization. NREL: Golden, CO, USA. Available online: https://www.nrel.gov/grid/solar-resource/spectra-am1.5.html (accessed on 27 March 2023).
39. Aranzaes, J.R.; Daniel, M.-C.; Astruc, D. Metallocenes as references for the determination of redox potentials by cyclic voltammetry—Permethylated iron and cobalt sandwich complexes, inhibition by polyamine dendrimers, and the role of hydroxy-containing ferrocenes. *Can. J. Chem.* **2006**, *84*, 288–299. [CrossRef]
40. Koops, S.E.; O'regan, B.C.; Barnes, P.R.F.; Durrant, J.R. Parameters Influencing the Efficiency of Electron Injection in Dye-Sensitized Solar Cells. *J. Am. Chem. Soc.* **2009**, *131*, 4808–4818. [CrossRef]
41. Hardin, B.E.; Snaith, H.J.; McGehee, M.D. The renaissance of dye-sensitized solar cells. *Nat. Photonics* **2012**, *6*, 162–169. [CrossRef]
42. Dessì, A.; Calamante, M.; Mordini, A.; Peruzzini, M.; Sinicropi, A.; Basosi, R.; de Biani, F.F.; Taddei, M.; Colonna, D.; di Carlo, A.; et al. Thiazolo[5,4-d]thiazole-based organic sensitizers with strong visible light absorption for transparent, efficient and stable dye-sensitized solar cells. *RSC Adv.* **2015**, *5*, 32657–32668. [CrossRef]
43. Wu, C.; Gong, Y.; Han, S.; Jin, T.; Chi, B.; Pu, J.; Jian, L. Electrochemical characterization of a novel iodine-free electrolyte for dye-sensitized solar cell. *Electrochim. Acta* **2012**, *71*, 33–38. [CrossRef]
44. Giribabu, L.; Bolligarla, R.; Panigrahi, M. Recent Advances of Cobalt(II/III) Redox Couples for Dye-Sensitized Solar Cell Applications. *Chem. Rec.* **2015**, *15*, 760–788. [CrossRef] [PubMed]
45. Bella, F.; Galliano, S.; Gerbaldi, C.; Viscardi, G. Cobalt-Based Electrolytes for Dye-Sensitized Solar Cells: Recent Advances towards Stable Devices. *Energies* **2016**, *9*, 384. [CrossRef]

46. Feldt, S.M.; Wang, G.; Boschloo, G.; Hagfeldt, A. Effects of Driving Forces for Recombination and Regeneration on the Photovoltaic Performance of Dye-Sensitized Solar Cells using Cobalt Polypyridine Redox Couples. *J. Phys. Chem. C* **2011**, *115*, 21500–21507. [CrossRef]
47. Cao, Y.; Liu, Y.; Zakeeruddin, S.M.; Hagfeldt, A.; Grätzel, M. Direct Contact of Selective Charge Extraction Layers Enables High-Efficiency Molecular Photovoltaics. *Joule* **2018**, *2*, 1108–1117. [CrossRef]
48. Sapp, S.A.; Elliott, C.M.; Contado, C.; Caramori, S.; Bignozzi, C.A. Substituted Polypyridine Complexes of Cobalt(II/III) as Efficient Electron-Transfer Mediators in Dye-Sensitized Solar Cells. *J. Am. Chem. Soc.* **2002**, *124*, 11215–11222. [CrossRef]
49. Klahr, B.M.; Hamann, T.W. Performance Enhancement and Limitations of Cobalt Bipyridyl Redox Shuttles in Dye-Sensitized Solar Cells. *J. Phys. Chem. C* **2009**, *113*, 14040–14045. [CrossRef]
50. Shavaleev, N.M.; Kessler, F.; Grätzel, M.; Nazeeruddin, M.K. Redox Properties of Cobalt(II) Complexes with Azole-Pyridines. *Inorg. Chim Acta* **2013**, *407*, 261–268. [CrossRef]